Special Issue

Radial Peripapillary Capillary Network Visualized Using Wide-Field Montage Optical Coherence Tomography Angiography

Tomoko Mase, Akihiro Ishibazawa, Taiji Nagaoka, Harumasa Yokota, and Akitoshi Yoshida

Department of Ophthalmology, Asahikawa Medical University, Asahikawa, Japan

Correspondence: Akihiro Ishibazawa, Department of Ophthalmology, Asahikawa Medical University, Midorigaoka Higashi 2-1-1-1, Asahikawa 078-8510, Japan; bazawa14@asahikawa-med.ac.jp.

TM and AI contributed equally to the work presented here and should therefore be regarded as equivalent authors.

Submitted: December 13, 2015
Accepted: June 19, 2016

Citation: Mase T, Ishibazawa A, Nagaoka T, Yokota H, Yoshida A. Radial peripapillary capillary network visualized using wide-field montage optical coherence tomography angiography. *Invest Ophthalmol Vis Sci*. 2016;57:OCT504–OCT510. DOI:10.1167/iovs.15-18877

Purpose. We quantitatively analyzed the features of a radial peripapillary capillary (RPC) network visualized using wide-field montage optical coherence tomography (OCT) angiography in healthy human eyes.

Methods. Twenty eyes of 20 healthy subjects were recruited. En face 3 × 3-mm OCT angiograms of multiple locations in the posterior pole were acquired using the RTVue XR Avanti, and wide-field montage images of the RPC were created. To evaluate the RPC density, the montage images were binarized and skeletonized. The correlation between the RPC density and the retinal nerve fiber layer (RNFL) thickness measured by an OCT circle scan was investigated.

Results. The RPC at the temporal retina was detected as far as 7.6 ± 0.7 mm from the edge of the optic disc but not around the perifoveal area within 0.9 ± 0.1 mm of the fovea. Capillary-free zones beside the first branches of the arterioles were significantly ($P < 0.0001$) narrower than those beside the second ones. The RPC densities at 0.5, 2.5, and 5 mm from the optic disc edge were 13.6 ± 0.8, 11.9 ± 0.9, and 10.4 ± 0.9 mm^{-1}. The RPC density also was correlated significantly ($r = 0.64$, $P < 0.0001$) with the RNFL thickness, with the greatest density in the inferotemporal region.

Conclusions. Montage OCT angiograms can visualize expansion of the RPC network. The RPC is present in the superficial peripapillary retina in proportion to the RNFL thickness, supporting the idea that the RPC may be the vascular network primarily responsible for RNFL nourishment.

Keywords: radial peripapillary capillary, optical coherence tomography, optical coherence tomography angiography

The radial peripapillary capillary (RPC) network is a unique vascular plexus in the retinal nerve fiber layer (RNFL); the capillaries run along relatively long straight paths and are limited to the posterior pole where they seem to be associated highly with the superficial nerve fibers.[1] The pathogenesis of glaucoma and most retinal vascular diseases may be related closely to this network, because several functional and structural changes represented by a Bjerrum scotoma, cotton-wool spots, and frame-shaped retinal hemorrhages match the distribution of this network.[2,3] Because understanding the features of the RPC network is important, histopathologic studies of the RPC in rhesus monkeys, cats, and human donor eyes have been performed.[1–3] However, evaluation of the RPC in living human eyes is limited even if using conventional fluorescein angiography.

Recently, several optical coherence tomography angiography (OCTA) methods have been developed and are gaining in popularity for three-dimensional noninvasive chorioretinal vascular imaging.[4–12] En face OCTA technology enables layer-by-layer evaluation of the chorioretinal vascular structures, allowing the RPC network to be visualized separately.[6] Using en face OCTA with application of the split-spectrum amplitude-decorrelation angiography algorithm, Spaide et al.[6] clearly showed wide-field montage images of the RPC network in the human retina for the first time. Yu et al.[9] quantitatively studied the RPC using speckle variance OCT (svOCT) and reported a positive correlation between the RPC density and RNFL thickness in the same healthy human eyes. Those authors also compared the morphologic characteristics and density of the RPC on en face svOCT images with histologic images in human donor eyes and showed that the en face OCTA technique using svOCT may be reliable for analyzing the RPC network in human retinas. However, in their svOCT studies, the field of view was small (636.5 μm^2), and the extent of the entire RPC network and the differences in the RPC in each retinal region were undetermined. In the current study, using wide-field montage OCTA, we analyzed quantitatively the features of the RPC network and the relationship between the RPC density and RNFL thickness in normal human eyes.

Methods

Study Population

Twenty eyes of 20 healthy volunteers (10 men, 10 women; average age, 30.5 ± 4.6 years) were recruited for this study. Eyes with high myopia (more than –6 diopters) were excluded. The study adhered to the tenets of the Declaration of Helsinki.

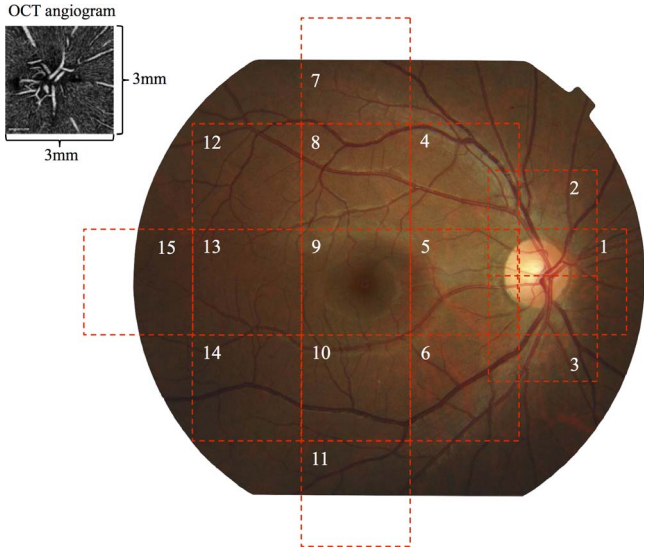

FIGURE 1. The regions from which montages of OCTA images are created. Fifteen 3 × 3-mm OCT angiograms are obtained. Two scans of the superior and inferior optic disc (nos. 2 and 3, respectively) are obtained using the Angio Disc mode. The other 13 scans of the posterior pole are obtained using the Angio Retina mode.

The institutional review board of Asahikawa Medical University approved the study. All subjects provided informed consent.

RPC Depiction and Creation of Wide-Field Montage OCT Angiograms

Subjects were imaged using the commercially available spectral-domain OCT (RTVue XR Avanti; Optovue, Inc., Fremont, CA, USA) with AngioVue software to obtain en face OCT angiograms as previously described.[10] The Avanti OCT provides 70,000 A-scans/second to acquire OCT angiograms consisting of 304 × 304 A-scans. Each OCT angiogram was created using orthogonal registration and merging of two consecutive scan volumes. Thirteen OCT angiograms (3 × 3 mm) were obtained using the Angio Retina mode in adjacent regions of the posterior pole by moving the software scanning area without changing fixation (Fig. 1), which was a modification of the method of de Carlo et al.[11] Two scans of the superior and inferior optic disc were obtained using the Angio Disc mode. The retina has multiple vascular planes.[6,13] The RPC network is the most superficial of the retinal vasculature and courses parallel to the nerve fibers. The ganglion cell layer has one or more capillary layers, which were referred to as the "inner retinal plexus" by Spaide et al.[6] The capillaries of the inner retinal plexus under the RPC network connected to the small branches of the retinal arterioles and venules, and their spread is obviously not in parallel with the nerve fibers. To depict the RPC network and minimize inclusion of the capillaries of the inner retinal plexus, the segmentation of the inner border was fixed at the vitreous cavity, and that of the outer border was moved down manually from the internal limiting membrane (ILM) toward the RNFL in the cross-sectional OCT B-scan with overlaying blood flow. The outer boundary on each OCT angiogram was determined at the layer that was just above the layer depicting the small branches of the retinal arterioles and venules that connect the capillaries of the inner retinal plexus (Fig. 2). The average depth of the outer border (in μm) from the ILM in each region to depict the RPC was calculated. ImageJ software (version 2.0.0-rc-41/1.50d; National Institutes of Health, Bethesda, MD, USA) with the plug-in MosaicJ (http://bigwww.epfl.ch/thevenaz/mosaicj/; in the public domain) then was used to automatically assemble the 3 × 3-mm OCT angiograms to create one wide-field montage OCT angiogram of the RPC network. Two graders (TM, AI) performed three measurements of the maximal distance (in mm) in the superior and inferior temporal retina from the edge of the optic disc and the minimal distance (in mm) from the fovea in which the RPC was observed on each montage OCT angiogram. The data were averaged, and the intraclass correlation coefficient (ICC) was calculated to assess the interexaminer reproducibility for both distance measurements. In all 20 enrolled eyes, three of the first and second branches of the retinal arterioles were manually selected on each montage OCT angiogram to measure the capillary-free zone (CFZ). The arteriolar branches that were not seen entirely on the OCT angiograms and/or side by side with the venules were not measured. The areas (mm^2) of the CFZ beside the first and second branches of the retinal arterioles in the 0.5 × 0.5-mm squares were measured. The areas of the CFZ obtained by two graders (TM, AI) were averaged.

Measurement of the RPC Density

We performed RPC densitometry using the publicly available software Fiji ImageJ (http://fiji.sc/Fiji; in the public domain)[14] as previously described[15] with some modification (Fig. 3). Signal noises of the montage images of the entire RPC network were removed using a bandpass filter (Fig. 3B). The montage image was converted to eight bits, and binarization was performed using Niblack's Auto Local Threshold (Fig. 3C).[16] The binarized image then was skeletonized (Fig. 3D). To analyze the RPC density 0.5, 2.5, and 5.0 mm from the optic disc edge, we selected the regions in which the RPC network was identified easily because the areas where the RPC was hard to detect had many false-positive pixels for this analysis. The selected regions of RPC densitometry are horseshoe-shaped in Figures 3A and 3E. Six 0.5 × 0.5-mm squares were chosen (Fig. 3E) to avoid including large vessels and the logo "angioflow," which could not be removed from the images. In the magnified skeletonized image (Fig. 3F), the lines were one pixel wide. Continuous lines were automatically displayed as orange pixels and bifurcation points as pink pixels. The terminals of the lines and one or two isolated pixels were automatically displayed as purple pixels. The RPCs have certain features that distinguish them from other retinal capillaries; that is, they run along relatively long straight paths and rarely anastomose with each other in their superficial location.[1] Therefore, we counted only the orange and pink pixels as the RPC. The RPC density was calculated by the formula (RPC density in mm^{-1}) = [(orange and pink pixels)(3/304)]/(area in mm^2). This calculation expressed the vessel density (in mm^{-1}) as the total vessel length per area.

RNFL Thickness Measurement

The Avanti OCT has built-in software, the ONH (optic nerve head) program, that calculates the circumpapillary RNFL thickness. We used this program to measure the average RNFL thickness in each of eight equally separated sectors along a circle with a diameter of 3.45 mm centered on the optic disc. The RPC densities in the same sectors also were calculated by the previously mentioned methods, but three 0.3 × 0.3-mm squares were used because the sectors were too narrow to use 0.5 × 0.5-mm squares.

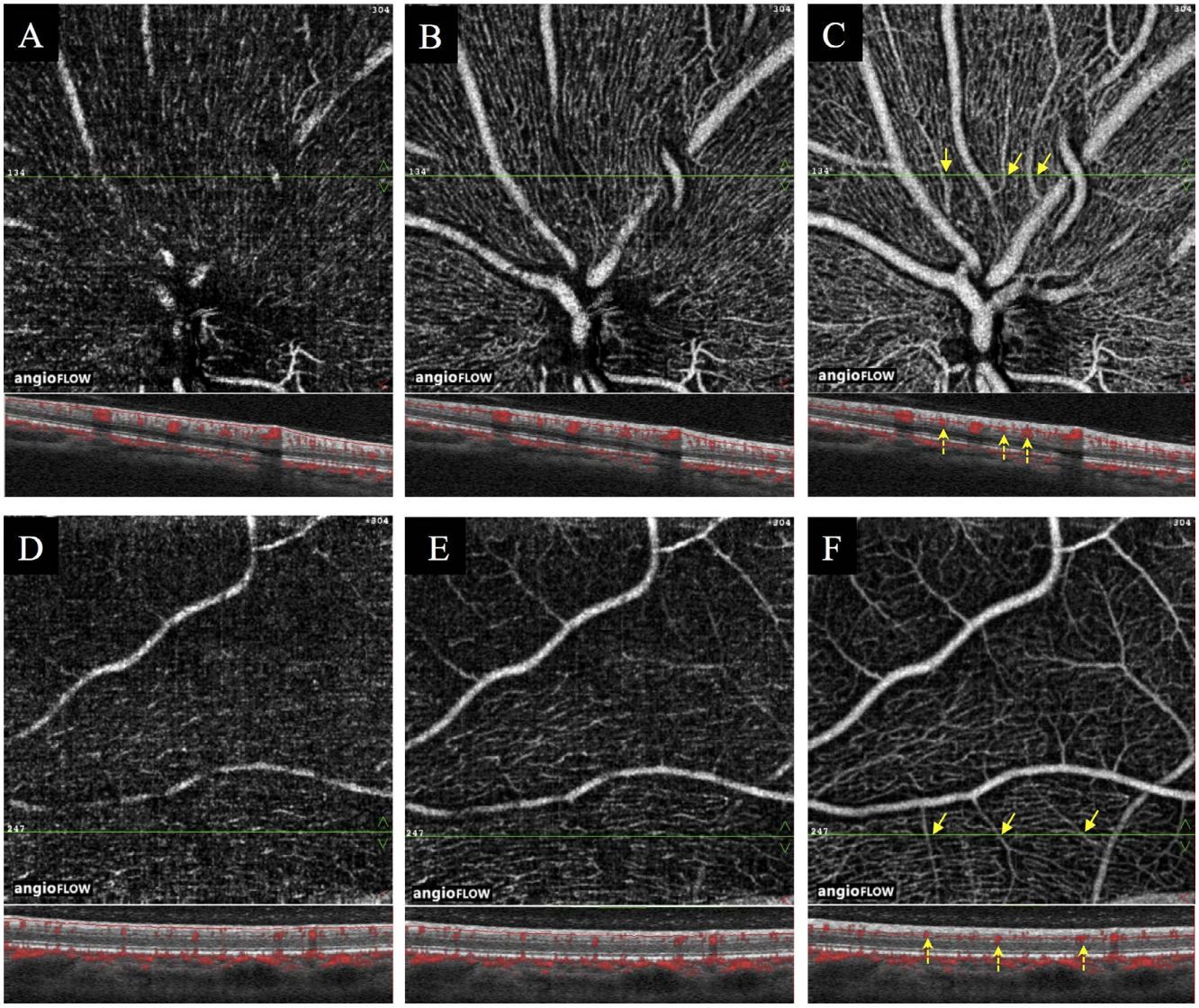

FIGURE 2. Determining the segmentation of the outer border on the en face OCT angiograms depicting the RPC network in the peripapillary (**A–C**) and peripheral superior temporal retina (**D**, **E**). The *green lines* on the en face OCT angiograms (*each top row*) indicate the position of the cross-sectional OCT B-scans with blood flow overlaid (*each bottom row*). The *red lines* on the OCT B-scan show the segmentation of the outer border of the en face OCT angiograms. The *yellow arrows* indicate the small branches of the retinal arterioles and venules; the *yellow dotted arrows* also indicate their blood flow signals overlaid on the B-scan. The segmentation of the inner border is fixed at the vitreous cavity, and that of the outer border is moved down manually from ILM toward the RNFL to minimize inclusion of the capillaries of the inner retinal plexus. The slabs of the different segmentation depths of the outer border in the same peripapillary scan are shown in (**A–C**). The outer segmentation borders are 40 μm (**A**), 72 μm (**B**), and 103 μm (**C**) beneath the ILM, respectively. We used slab B to create the montage of OCT angiograms, because B does not include the small branches (*yellow arrows*) that generate inner retinal plexuses. In the same manner, the slabs of the different segmentation depths of the outer border in the same peripheral temporal scan are shown in (**D–F**). The outer segmentation border is 30 μm (**D**), 47 μm (**E**), and 85 μm (**F**) beneath the ILM, respectively. We used slab E to create the montage OCT angiogram.

Statistical Analysis

All values were expressed as the mean ± standard deviation. Kolmogorov-Smirnov test revealed the data of the RPC densities, and the CFZ areas were parametric. The unpaired *t*-test was used to compare the areas of the CFZ beside the first branch of the retinal arteriole and those beside the second branch. The difference in the RPC density at each distance from the optic disc edge was assessed by 1-way analysis of variance followed by the Tukey's post hoc test. Correlations between the RNFL thickness and the RPC density were analyzed using Pearson's correlation model. All statistical analyses were performed with EZR (Easy R) Package (Saitama Medical Center, Jichi Medical University, Saitama, Japan), which is a graphic user interface for R (The R Foundation for Statistical Computing, Vienna, Austria). More precisely, it is a modified version of R commander designed to add statistical functions frequently used in biostatistics.[17] $P < 0.05$ was considered significant.

RESULTS

Depiction of the RPC Network

Figure 4 shows each segmentation depth of the outer border to depict the RPC on en face OCT angiograms, which was manually moved toward the RNFL at different depths to just

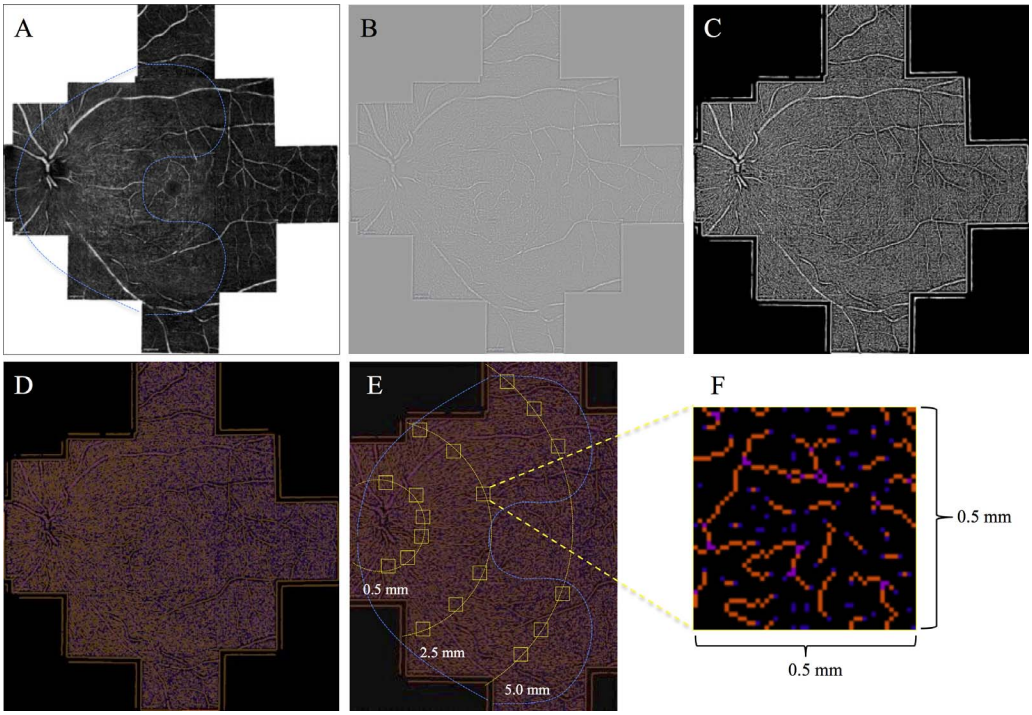

FIGURE 3. (**A**) A montage OCT angiogram of the RPC network and (**B**–**F**) converted images in a normal healthy eye. The *blue horseshoe-shaped regions* in (**A**) and (**E**) indicate the regions selected for densitometry. (**B**) Using ImageJ software, the signal noises of the montage images are removed using a bandpass filter. (**C**) The montage image is converted to eight bits, and binarization is performed using Niblack's Auto Local Threshold. (**D**) The binarized image is skeletonized. (**E**) To analyze the RPC density at each distance (0.5, 2.5, and 5.0 mm) from the optic disc edge, six 0.5 × 0.5-mm squares are selected. (**F**) In the magnified image, the lines are one pixel wide. Continuous lines are automatically displayed as orange pixels, and bifurcation points as pink pixels. The terminals of the lines and one or two isolated pixels are purple. We counted only the orange and pink pixels, and the RPC density in the square is calculated by the formula (RPC density in mm^{-1}) = [(orange and pink pixels)(3/304)]/(area in mm^2). For example, the square in (**F**) has 246 orange, and 30 pink pixels. Therefore, the RPC density is calculated as [(246+30)(3/304)]/0.25 = 10.9 (mm^{-1}).

before the inner retinal plexus. The segmentation depth gradually decreased from the peripapillary region to the peripheral temporal region; the RPC network of the peripapillary retina could be depicted within the deeper RNFL than that of the peripheral retina. The RPC was not depicted in the temporal macula. A wide-field montage OCT angiogram of the entire RPC network is shown in Figure 5A. The RPC at the temporal retina was detected as far as 7.6 ± 0.7 mm from the edge of the optic disc but not around the perifoveal area within 0.9 ± 0.1 mm of the fovea. The ICC was 0.82 (95% confidence interval [CI], 0.45–0.92) for the interexaminer reproducibility of the maximal-distance measurements and 0.54 (95% CI, 0.29–0.72) for that of the minimal-distance measurements. Almost perfect reproducibility was observed for the former but moderate reproducibility for the latter.

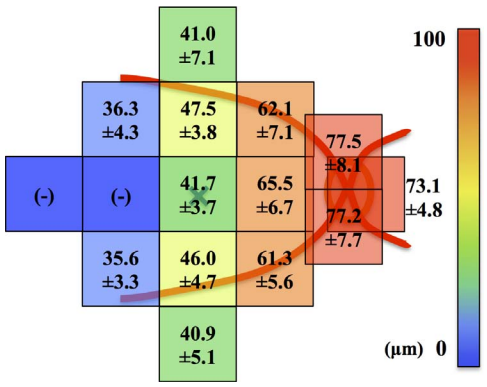

FIGURE 4. The segmentation depth of each region to depict the RPC. The segmentation depth of the outer border to depict the RPC on en face OCT angiograms, which is manually moved toward the RNFL at different depths to just before the inner retinal plexus, decreases gradually from the peripapillary region to the peripheral temporal region. The RPC is not depicted in the temporal macula. The values (μm) are expressed as the means ± standard deviations.

CFZs Beside the Arterioles

When focusing on the RPC near the large vessels, narrow spaces were seen beside the arterioles but not the venules where the RPC was not depicted (Fig. 5A), which we referred to as CFZs. Magnified OCT angiograms near the first branch of an arteriole (Fig. 5B) and a second branch (Fig. 5C) enabled measurement of the areas of the CFZs. The average CFZ beside the second branches (0.070 ± 0.009 mm^2) was significantly ($P < 0.0001$) larger than that beside the first branches (0.050 ± 0.007 mm^2).

RPC Density

Using binarized and skeletonized OCT angiograms, the RPC density was evaluated quantitatively. The RPC densities were 13.6 ± 0.8, 11.9 ± 0.9, and 10.4 ± 0.9 mm^{-1}, respectively, at 0.5, 2.5, and 5 mm from the optic disc edge. The densities decreased significantly ($P < 0.0001$) with increasing distance from the temporal side of the optic disc (Table). We also investigated the correlation between the RNFL thickness and RPC density around the optic disc. The circumpapillary RNFL thickness along a circle with a diameter of 3.45 mm centered

Table. Density of the Radial Peripapillary Capillary Network

Distance From the Disc	0.5 mm	2.5 mm	5 mm
Density, mm^{-1}	13.6 ± 0.8	11.9 ± 0.9	10.4 ± 0.9

on the optic disc had bimodal peaks at superior and inferior temporal sectors (Fig. 6B). The RPC density along the same circle also had bimodal peaks in the same manner as the RNFL thickness around the optic disc (Fig. 6E). The RPC density was significantly ($P < 0.0001$) proportionally correlated with the RNFL thickness ($r = 0.64$).

Discussion

Wide-field montage OCT angiograms show the retinal vasculature in greater detail than single-scan 8 × 8-mm OCT angiograms by combining the 3 × 3-mm scans.[11] The current study showed that wide-field montage OCT angiograms visualized the extent of the entire RPC network and for the first time evaluated quantitatively the distribution of the RPC in healthy living human eyes. The RPC spreads as far as approximately 8 mm from the temporal edge of the optic disc (Fig. 5A). Moreover, the finding that the RPC was not detected around an area of approximately 1 mm in the perifovea agreed with a previous anatomic observation.[1]

The current study also found that the features of the RPC varied from one retinal area to another. The segmentation depth to depict the RPC on OCT angiograms gradually decreased from the peripapillary region to the peripheral temporal region (Fig. 4). The RPC density decreased in a distance-dependent manner from the temporal side of the optic disc (Table). The current findings, therefore, indicated that the RPCs in the peripapillary retina are denser and located within thicker RNFL than in the peripheral retina. Those results agreed with histologic studies performed by Yu's group.[3,9,12] Those authors found that in human donor eyes the RPC density decreased significantly with increasing distance from the optic disc edge,[3] that the RPC density was significantly higher in the arcuate regions (superior temporal [ST] and inferior temporal [IT]) than in the other quadrants, and that the RPC volume generally was correlated positively with the RNFL thickness.[3] In the current study, we measured the RNFL thickness in healthy living eyes using the ONH program and found that the RNFL thickness and RPC density along a circle with a diameter of 3.45 mm centered on the optic disc had bimodal peaks at the ST and IT sectors (Figs. 6B, 6E). Yu et al.[9] also analyzed en face svOCT images (areas of 636.5 μm^2) acquired from healthy volunteers and reported that

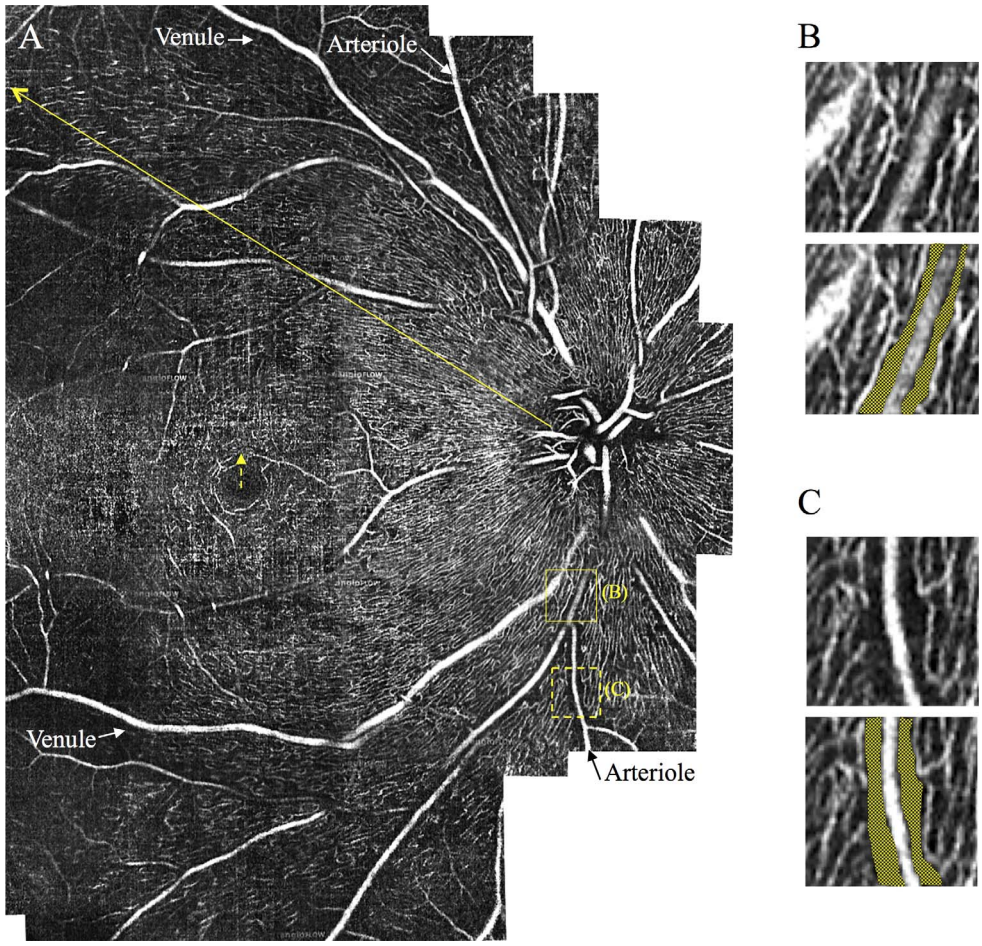

Figure 5. A wide-field montage OCT angiogram of the RPC network in the same eye shown in Figure 1. (**A**) A *yellow arrow* and a *yellow dashed arrow*, respectively, show the maximal distance from the edge of the optic disc and the minimal distance from the fovea in which the RPC network is seen. (**B**, **C**) The *top rows* show magnified images of 0.5 × 0.5-mm *yellow* and *yellow-dashed squares* in (**A**). (**B**) A first branch of an arteriole and (**C**) a second branch have CFZs beside them where the RPC is not depicted. The *bottom rows* show manually traced CFZs beside the arterioles. The areas of the CFZs beside the first and second branches are 0.044 and 0.066 mm^2, respectively.

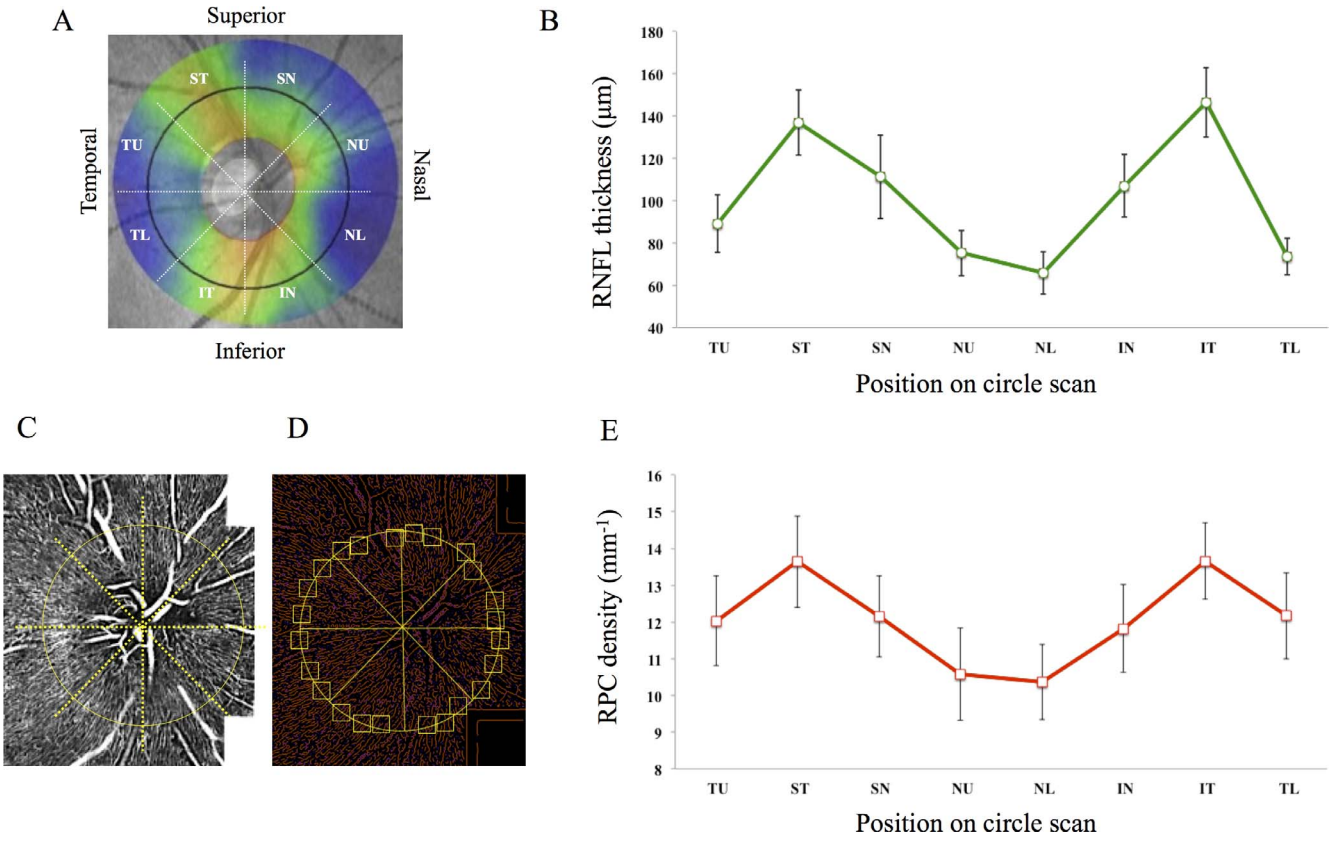

Figure 6. The RNFL thickness and RPC density around the optic disc. (**A**) The circumpapillary RNFL thickness along a circle with a diameter of 3.45 mm centered on the optic disc is measured using the ONH program built into the Avanti OCT. The averaged RNFL thickness separated into eight sectors is calculated. The sectors are the temporal upper (TU), superior temporal (ST), superior nasal (SN), nasal upper (NU), nasal lower (NU), inferior nasal (IN), inferior temporal (IT), and temporal lower (TL). (**B**) The RNFL thickness has bimodal peaks at ST and IT; the thickest sector is IT. (**C**) The RPC density along the same circle with a diameter of 3.45 mm centered on the optic disc is measured. (**D**) A binarized and skeletonized image from (**C**). Three 0.3×0.3-mm squares in each sector are chosen for RPC densitometry. (**E**) The RPC density also has bimodal peaks in the same manner as the RNFL thickness around the optic disc.

the RPC densities in the ST and IT regions were significantly higher than in the superior and/or inferior regions. The current results agreed with theirs, and we also showed that the RPC density was significantly and proportionally correlated with the RNFL thickness ($r = 0.64$) in healthy living eyes.

This proportional relationship between the RNFL thickness and RPC density closely resembled that between the RNFL thickness and hyperreflective bundle width, that is, the nerve fiber bundle width, observed by adaptive optics scanning laser ophthalmoscopy. Takayama et al.[18] reported that the distribution of the nerve fiber bundle width around the disc had a double peak, as did that of the RNFL thickness evaluated by a circle scan around the optic disc seen on OCT images; and the RNFL thickness was correlated positively with the nerve fiber bundle width. When considered together with the current results, the thicker RNFL has a wider nerve fiber bundle and denser RPCs, suggesting that the RPC may be the vascular network that is primarily responsible for RNFL nourishment.

Wide-field montage OCTA clearly visualized the CFZs beside the retinal arterioles (Fig. 5A). However, the retinal venules did not have CFZs, and dense RPCs near the venules were observed. To the best of our knowledge, no OCTA study has reported the presence of CFZs in healthy and diseased eyes. A previous observation using retinas injected with India ink showed that the radial capillaries only occasionally crossed major retinal arterial branches and appeared to arise independently from arterioles on either side of the arteriolar trunk.[1] Except for the points at which the capillaries arose from the arterioles, the arterioles had CFZs. We showed quantitatively for the first time that the CFZs beside the first branches of retinal arterioles were narrower than those beside the second branches. The results may be related to structural differences between the first and second branches of the arterioles. Larger arterioles have a larger area of endothelial layer and a thicker smooth muscle layer than smaller arterioles; the larger arterioles themselves consume certain amounts of oxygen, and the diffusion of oxygen may be restricted.[19,20] Therefore, the CFZs beside the first branches may be narrower in order to oxygenate the adjacent retinal tissues. Because changes in the retinal oxygen saturation in retinal vascular disorders have been reported,[21–24] the CFZs may change. Further studies are needed to elucidate the features of the CFZs.

The current study had some limitations. First, we obtained 15 OCT angiograms to create a wide-field montage, but all the images were not perfectly aligned with each other because the posterior pole curves slightly (e.g., inferior temporal retinal arterioles and venules in Fig. 5A). The current study did not include highly myopic eyes, and moreover, the misalignment occurred in the peripheral regions; therefore, there was little effect on the results. Second, creating the wide-field montage images is time-consuming. The 6×6- and 8×8-mm single scans do not have sufficient resolution to evaluate the changes in the RPC networks in patients with retinal vascular diseases. In clinical use, we do not obtain 15 series of 3×3-mm OCT angiograms from patients. Development of advanced OCTA with higher resolution, a wider scan area, and faster scan speed

is expected. Third, we manually, not automatically, moved the outer segmentation border down from the ILM toward the RNFL in the cross-sectional OCT B-scans with overlaying blood flow to depict the RPC on the en face OCT angiograms as selectively as possible, because automatic segmentation cannot minimize the depiction of the capillaries from the inner retinal plexus. Although there was some noise from the capillaries of the inner retinal plexus, we identified the RPC network that coursed parallel to the nerve fibers in the peripheral temporal retina (Fig. 5A). However, in the macular en face OCT angiograms, the noise from the capillaries in the inner retinal plexus was unavoidable because the RNFL near the fovea was converted to Henle's fiber layer, so the uniform segmentation depth of the outer border down from the ILM included the perifoveal ganglion cell layer and inner plexiform layer (Fig. 5A). This is because the reproducibility of the minimal-distance measurement of the RPC from the fovea was less than that for the maximal-distance measurement. Further improvements in high-resolution and precise segmentation on OCTA might facilitate more detailed observation of the RPC network near the fovea.

In conclusion, montage OCTA can clearly visualize the expansion of the RPC network, which is distributed to the superficial peripapillary retina relative to the RNFL thickness. The current results of the density and extent of the RPCs in healthy eyes can be considered as a standardized map of the RPC network and compared to those in eyes with retinal vascular disorders.

Acknowledgments

Supported by Grant-in-Aid for Scientific Research (B) 25293352 (TN) from the Ministry of Education, Science, and Culture, Tokyo, Japan.

Disclosure: **T. Mase**, None; **A. Ishibazawa**, None; **T. Nagaoka**, None; **H. Yokota**, None; **A. Yoshida**, None

References

1. Henkind P. Radial peripapillary capillaries of the retina. I. Anatomy: human and comparative. *Br J Ophthalmol*. 1967;51:115–123.
2. Alterman M, Henkind P. Radial peripapillary capillaries of the retina. II. Possible role in Bjerrum scotoma. *Br J Ophthalmol*. 1968;52:26–31.
3. Yu PK, Cringle SJ, Yu DY. Correlation between the radial peripapillary capillaries and the retinal nerve fibre layer in the normal human retina. *Exp Eye Res*. 2014;129:83–92.
4. Huang Y, Zhang Q, Thorell MR, et al. Swept-source OCT angiography of the retinal vasculature using intensity differentiation-based optical microangiography algorithms. *Ophthalmic Surg Lasers Imaging Retina*. 2014;45:382–389.
5. Schwartz DM, Fingler J, Kim DY, et al. Phase-variance optical coherence tomography: a technique for noninvasive angiography. *Ophthalmology*. 2014;121:180–187.
6. Spaide RF, Klancnik JM Jr, Cooney MJ. Retinal vascular layers imaged by fluorescein angiography and optical coherence tomography angiography. *JAMA Ophthalmol*. 2015;133:45–50.
7. Jia Y, Bailey ST, Hwang TS, et al. Quantitative optical coherence tomography angiography of vascular abnormalities in the living human eye. *Proc Natl Acad Sci U S A*. 2015;112:E2395–E2402.
8. Miura M, Hong YJ, Yasuno Y, Muramatsu D, Iwasaki T, Goto H. Three-dimensional vascular imaging of proliferative diabetic retinopathy by Doppler optical coherence tomography. *Am J Ophthalmol*. 2015;159:528–538, e523.
9. Yu PK, Balaratnasingam C, Xu J, et al. Label-free density measurements of radial peripapillary capillaries in the human retina. *PLoS One*. 2015;10:e0135151.
10. Ishibazawa A, Nagaoka T, Takahashi A, et al. Optical coherence tomography angiography in diabetic retinopathy: a prospective pilot study. *Am J Ophthalmol*. 2015;160:35–44, e31.
11. de Carlo TE, Salz DA, Waheed NK, Baumal CR, Duker JS, Witkin AJ. Visualization of the retinal vasculature using wide-field montage optical coherence tomography angiography. *Ophthalmic Surg Lasers Imaging Retina*. 2015;46:611–616.
12. Tan PE, Balaratnasingam C, Xu J, et al. Quantitative comparison of retinal capillary images derived by speckle variance optical coherence tomography with histology. *Invest Ophthalmol Vis Sci*. 2015;56:3989–3996.
13. Weinhaus RS, Burke JM, Delori FC, Snodderly DM. Comparison of fluorescein angiography with microvascular anatomy of macaque retinas. *Exp Eye Res*. 1995;61:1–16.
14. Schindelin J, Arganda-Carreras I, Frise E, et al. Fiji: an open-source platform for biological-image analysis. *Nat Methods*. 2012;9:676–682.
15. Nemiroff J, Kuehlewein L, Rahimy E, et al. Assessing deep retinal capillary ischemia in paracentral acute middle maculopathy by optical coherence tomography angiography. *Am J Ophthalmol*. 2016;162:121–132, e121.
16. Sonoda S, Sakamoto T, Yamashita T, et al. Choroidal structure in normal eyes and after photodynamic therapy determined by binarization of optical coherence tomographic images. *Invest Ophthalmol Vis Sci*. 2014;55:3893–3899.
17. Kanda Y. Investigation of the freely available easy-to-use software "EZR" for medical statistics. *Bone Marrow Transplant*. 2013;48:452–458.
18. Takayama K, Ooto S, Hangai M, et al. High-resolution imaging of the retinal nerve fiber layer in normal eyes using adaptive optics scanning laser ophthalmoscopy. *PLoS One*. 2012;7:e33158.
19. Takahashi T. *Microcirculation in Fractal Branching Networks*. Tokyo: Springer Japan; 2014:47–69.
20. Shibata M, Qin K, Ichioka S, Kamiya A. Vascular wall energetics in arterioles during nitric oxide-dependent and -independent vasodilation. *J Appl Physiol*. 2006;100:1793–1798.
21. Hardarson SH, Stefansson E. Oxygen saturation in branch retinal vein occlusion. *Acta Ophthalmol*. 2012;90:466–470.
22. Hardarson SH, Stefansson E. Retinal oxygen saturation is altered in diabetic retinopathy. *Br J Ophthalmol*. 2012;96:560–563.
23. Tayyari F, Khuu LA, Flanagan JG, Singer S, Brent MH, Hudson C. Retinal blood flow and retinal blood oxygen saturation in mild to moderate diabetic retinopathy. *Invest Ophthalmol Vis Sci*. 2015;56:6796–6800.
24. Eliasdottir TS, Bragason D, Hardarson SH, Kristjansdottir G, Stefansson E. Venous oxygen saturation is reduced and variable in central retinal vein occlusion. *Graefes Arch Clin Exp Ophthalmol*. 2015;253:1653–1661.

Investigative Ophthalmology & Visual Science